Environ. Sci. Technol. **1999**, *33,* 2224−2233

Local Motions of Organic Pollutants in Soil Components, as Studied by ^{2}H NMR

JINCHENG XIONG, HERMAN LOCK, I-SSUER CHUANG, CAMILLE KEELER, AND GARY E. MACIEL*

Department of Chemistry, Colorado State University, Fort Collins, Colorado 80523

^{2}H NMR spectra and interpretations are presented on a series of samples, each consisting of a deuterium-labeled organic pollutant (trichloroethylene, acetone, pyridine, benzene, or ethylene glycol) adsorbed on a soil component (montmorillonite clay or humic acid). Spectra were obtained over a wide temperature range and using two values of the quadrupolar echo delay period. Computer simulations of line shapes resulting from various forms of local motion of C−^{2}H moieties provide useful guidelines for interpreting the experimental results. In a few cases, detailed line shape simulations are given. This approach is attractive for elucidation of the detailed motional behaviors of organic pollutants adsorbed in soil.

Introduction

Knowledge of the fundamental chemical−physical behaviors of pollutant species in soil/groundwater systems is prerequisite to an accurate prediction of the fates of these species in the environment (e.g., long-term sequestering, chemical transformation, complexation, release to groundwater, etc.) or to the design of effective remediation strategies. One aspect of understanding this fundamental behavior and a potentially valuable property for characterizing the environmental fate of an organic pollutant is the degree and precise nature of whatever local mobility/motion is manifested by the pollutant species adsorbed in a soil system. For example, a pollutant species that interacts strongly with certain regions of a clay will certainly manifest a more constrained and lower local mobility than if the same species were not interacting at all with "solid" soil substrates; an intermediate degree and nature of local motion/mobility would be expected for a pollutant species loosely interacting in a physiosorbed manner with a silica component in soil. Indeed, one might hope that, if the local pollutant motion in a sample of pollutant adsorbed on a whole soil can be recognized as resembling that of the same pollutant adsorbed on one type of major soil component (e.g., clay, silica, humic acid, fulvic acid, humin), this recognition may provide one type of indicator of where (in which component) in a complex soil a specific pollutant is located and in what motional state.

^{2}H NMR line shapes, based on the nuclear electric quadrupole effect of the spin-1 ^{2}H nuclide, have long been recognized as a powerful method for elucidating the detailed nature of local mobility of the C−D ≡ C−^{2}H bond in an organic species with the required ^{2}H labeling (*1*−*6*). In the limit in which the magnitude of the nuclear electric quadrupole interactions of ^{2}H in such systems (typically <200 kHz) is much smaller than the ^{2}H Larmor (resonance) frequency (92.17 MHz in the present case), the quadrupole interaction is treated as a first-order perturbation. In this case, the nuclear electric quadrupole effect is given by

$$\upsilon_Q = \pm \frac{3}{8}\frac{e^2qQ}{h}(3\cos^2\theta - 1 - \eta\sin^2\theta\cos 2\phi) \quad (1)$$

where eQ is the "nuclear electric quadrupole moment" (a fixed property of ^{2}H); $eq \equiv (\partial^2V/\partial Z^2)_0$ is a property of the local electric field environment in which the ^{2}H nucleus is situated (**V** is the so-called electric field gradient tensor in its principal axis system, X, Y, Z, eq being its largest component), and $\eta \equiv \{(\partial^2V/\partial X^2)_0 - (\partial^2V/\partial Y^2)_0\}/(eq)$ is called the asymmetry parameter. In eq 1, θ is the angle between the Z axis and the direction (z) of the static magnetic field ($\mathbf{B_0}$), and ϕ is a second angle relating the two relevant axis systems (x, y, z and X, Y, Z). A spectral parameter that is often useful in the NMR of quadrupolar nuclei is the quadrupole coupling constant, defined by $Q_{CC} = e^2qQ/h$.

For a powder or amorphous sample, the $[3\cos^2\theta - 1 - \eta\sin^2\theta\cos^2\phi]$ factor is summed over all initial orientations and averaged over all transient orientations if the molecule is in motion. The two resonance positions represented by the ± in eq 1 manifest the fact that there are two resonance "peaks" (contributions) for each θ,ϕ combination, corresponding to $\Delta m = -1 \leftrightarrow 0$ and $\Delta m = 0 \leftrightarrow 1$, where m is the I_z quantum number. To a reasonable level of approximation, the static electric field gradient tensor relevant to C−^{2}H units in typical organic species can be taken to be axially symmetric, i.e., with $\eta = 0$. This yields eq 2, which is the form we used throughout the work described in this paper:

$$\upsilon_Q = \pm \frac{3}{8}\frac{e^2qQ}{h}(3\cos^2\theta - 1) \quad (2)$$

The ^{2}H NMR pattern of a powder sample consisting of a collection of randomly oriented, static crystallites has a contribution for each crystallite orientation (each value of θ) weighted according to random statistics. The resulting line shape is the classic "Pake pattern," with a full width of about 250 kHz. The same pattern results from an amorphous solid with no molecular level motion. In the presence of motion, this pattern is narrowed in a manner that depends in detail on the nature of the motion. Hence, the resultant, observed ^{2}H NMR pattern is exquisitely sensitive to the details that characterize the local motion. In the limit of rapid isotropic motion, the very broad (e.g., 250 kHz) ^{2}H pattern of a static system is narrowed to the sharp peak characteristic of a liquid sample. The usual ^{2}H NMR strategy for elucidating local C−D motion is to compare experimentally determined ^{2}H line shapes with patterns that are simulated by computer calculations based on spin-dynamics calculations that take individual or composite motional models explicitly into account.

It is customary to make the ^{2}H NMR measurements over a substantial temperature range, not necessarily because the system is of intrinsic interest over a broad temperature range, but for the following two reasons: (i) Examining ^{2}H NMR patterns over a broad temperature range often facilitates the identification of rapid and difficult-to-recognize motions that occur at the high end of the temperature range by tracking the more easily identified patterns of slower motion on the lower side of the temperature range into the narrower patterns that typically occur at higher temperatures. This point will

* Corresponding author phone: (970)491-6480; fax: (970)491-1801; e-mail: maciel@lamar.colostate.edu.

10.1021/es981221w CCC: $18.00
Published on Web 05/20/1999

be more apparent in the ^2H NMR patterns displayed below. (ii) By obtaining the rates of a motion as a function of temperature, one can compute the activation energy for that motion, a parameter that can provide both predictive capabilities and chemical/structural insight regarding a pollutant/matrix interaction.

This paper provides a brief, preliminary survey of an extensive long-term ^2H NMR study of local motion of certain organic pollutants adsorbed on specific soil components as well as intact soil. The specific organic pollutants included in this survey are isotopically labeled ethylene glycol, trichloroethylene, benzene, acetone, and pyridine. Apparently there have been very few such studies on pollutant/soil systems published previously.

Experimental Section

The ^2H-labeled compounds were obtained from Cambridge Isotopes. The Ca-montmorillonite was obtained from the Missouri Clay Repository, Columbia, MO. The humic acid was isolated from a soil collected in the Uncompahgre National Forest of southwestern Colorado. Details of the separation and characterization of this humic acid will be given elsewhere (*7*). Most of the samples of organic pollutants adsorbed on (in) soil components were prepared by either (i) gas-phase adsorption of a highly volatile organic species on to a soil component in a vacuum line or (ii) mixing a pentane slurry of the soil component with a pentane solution of the organic pollutant, decanting the supernatant pentane phase, and drying the residue at 10^{-3} Torr at 25 °C for 4 h. For the $HOCD_2CD_2OH$/humic sample, H_2O was removed from a slurry of the humic sample with an aqueous $HOCD_2$-CD_2OH solution under vacuum (10^{-3} Torr) at 25 °C.

^2H NMR spectra were obtained at 92.17 MHz using either (i) a Bruker AM-600 spectrometer that was modified for wide-line ^2H NMR spectroscopy by the addition of a 1000-W rf amplifier, a home-built high-speed digitizer (1 complex data point/0.3 μs), and a home-built probe or (ii) the same configuration except based on a Chemagnetics Infinity-600 console. The quadrupole-echo technique (*8*, *9*) was used to record all ^2H spectra, typically in two sets of experiments with pulse spacing periods, $t_q = 40$ μs and $t_q = 100$ μs. A spectral width of 1−3 MHz was typically used to obtain each ^2H spectrum.

^2H line-shape simulations were based on the MXET1 version of the MXQET program (*10*), kindly provided by R. R. Vold. The calculated free induction decays were multiplied, prior to Fourier transformation, by the same experimental weighting functions as used in obtaining the experimental spectra.

Results and Discussion

^2H Line Shape Simulations. To provide some qualitative insights into the dependence of ^2H NMR line shapes for those who may not be familiar with the ^2H NMR approach, we have carried out a series of computer calculations (simulations) of ^2H NMR line shapes on C−D groups that undergo motion according to specific motional models at specific rates. These calculations were based on well-established density-matrix methodology, using an available computer program (*10*). For each simulation, each ^2H line shape pattern is "powder summed", reflecting the random orientations of an amorphous material, such as soil substrates. Figure 1 shows ^2H NMR line shape simulations for $C-^2H \equiv C-D$ groups, with $Q_{cc} = 180$ kHz, executing a variety of types of motion, as indicated for the following specific values chosen for motional reorientation correlation times, τ_r: 1000, 30, 3, 0.3, 0.03, and 0.001 μs. The simulations in Figure 1 were carried out for two different values (40 and 100 μs, corresponding to the upper trace and lower, dashed trace of each pair, respectively) of the pulse spacing periods t_q employed in the quadrupolar echo technique that is commonly used for such measurements (*8*, *9*), including those of this study. These kinds of patterns are useful for providing qualitative guidelines regarding the types of motions that can be responsible for specific, observed ^2H NMR patterns. It should be noted that for all of the simulated ^2H line shapes given in this paper, the maximum vertical intensity of each simulation for $t_q = 40$ μs is arbitrarily scaled to the same height, and the corresponding line shape simulated for $t_q = 100$ μs is scaled relative to the $t_q = 40$ μs case.

For each type of motion represented in Figure 1, the fastest motion ($\tau_r = 0.001$ μs) represents the approach to the fast motion limit, $\tau_r \rightarrow 0$. For the slowest motions (largest reorientational correlation time, 10^3 μs), each type of motion is expected to yield essentially an unaveraged, classic "Pake powder pattern" (*1*, *2*). In this pattern, one sees maxima at the "horns", which occur at $\pm 3Q_{cc}/8$ ($\pm$67.5 kHz for $Q_{cc} =$ 180 kHz) and lower-intensity discontinuities at $\pm 3Q_{cc}/4$ ($\pm$135 kHz for $Q_{cc} =$ 180 kHz). One sees the most efficient averaging/narrowing of the Pake powder pattern for the isotropic reorientation case (Figure 1a), for which the $\tau_r = 0.001$ μs simulation yields the completely averaged, liquidlike narrow peak. Although not shown in Figure 1, it is clear that any motion that leaves the orientation of the C−D axis unchanged will give rise to no averaging/narrowing of the Pake powder pattern. Such motions would include any rotation or jump motion about the C−D axis and 180° rotational jump motion about an axis perpendicular to the C−D bond (which reverses the direction of the C−D bond but leaves the C−D axis unchanged).

The actual input parameters for the line shape simulation calculations are *not* the averaged reorientational correlation times (τ_r) represented in Figure 1, but rather the rate constants, k_j, in terms of which we define the corresponding motional jump correlation times, $\tau_j = k_j^{-1}$, which are the time intervals between jumps among the different C−D orientations, or sites, in a specific motional simulation model. Only a finite number of sites can be used in the numerical simulation of a motion such as isotropic reorientation or rotational diffusion. In practice, the number of sites used in such simulations is chosen typically to be the minimum number that produces essentially the same simulated ^2H NMR line shape as in analogous simulations with more sites. In the simulation of rotational diffusion, a simulation based on say 36 sites with a jump correlation time of τ_j of X μs would produce nearly the same ^2H line shape as if a τ_j value of $X/10$ μs had been used in an analogous simulation based on 360 sites. It could be misleading to compare the line shape from a 360-site simulation with the line shape obtained from a corresponding 36-site simulation *with the same value of* τ_j. For modeling isotropic reorientation in this study, τ_j specifies the time during which a specific C−D moiety jumps from any one of the $n = 32$ specific orientations used in the simulation to *all* 31 other orientations. In contrast, for each of the other motional models, a specific τ_j value specifies the time during which a specific C−D moiety jumps to each of its *two* neighboring orientations or, in the case of motional model b′, to its *one* neighboring orientation.

The most direct comparison of simulations based on motional models with different numbers of sites can be made if one uses a common definition of a motional correlation time, τ_r, that in some appropriate way "normalizes" different motional models with respect to the number of jumps. For this purpose, we use a correlation time τ_r, which we *define* as the "average" time required for a *total* angular excursion by one radian; i.e., $\tau_r = \tau_j/\sum_i|\theta_i|$), where the sum of jump angles, $\sum_i|\theta_i|$, is over all the stepwise jumps that occur (on the average) during τ_j in a specific motional model. While

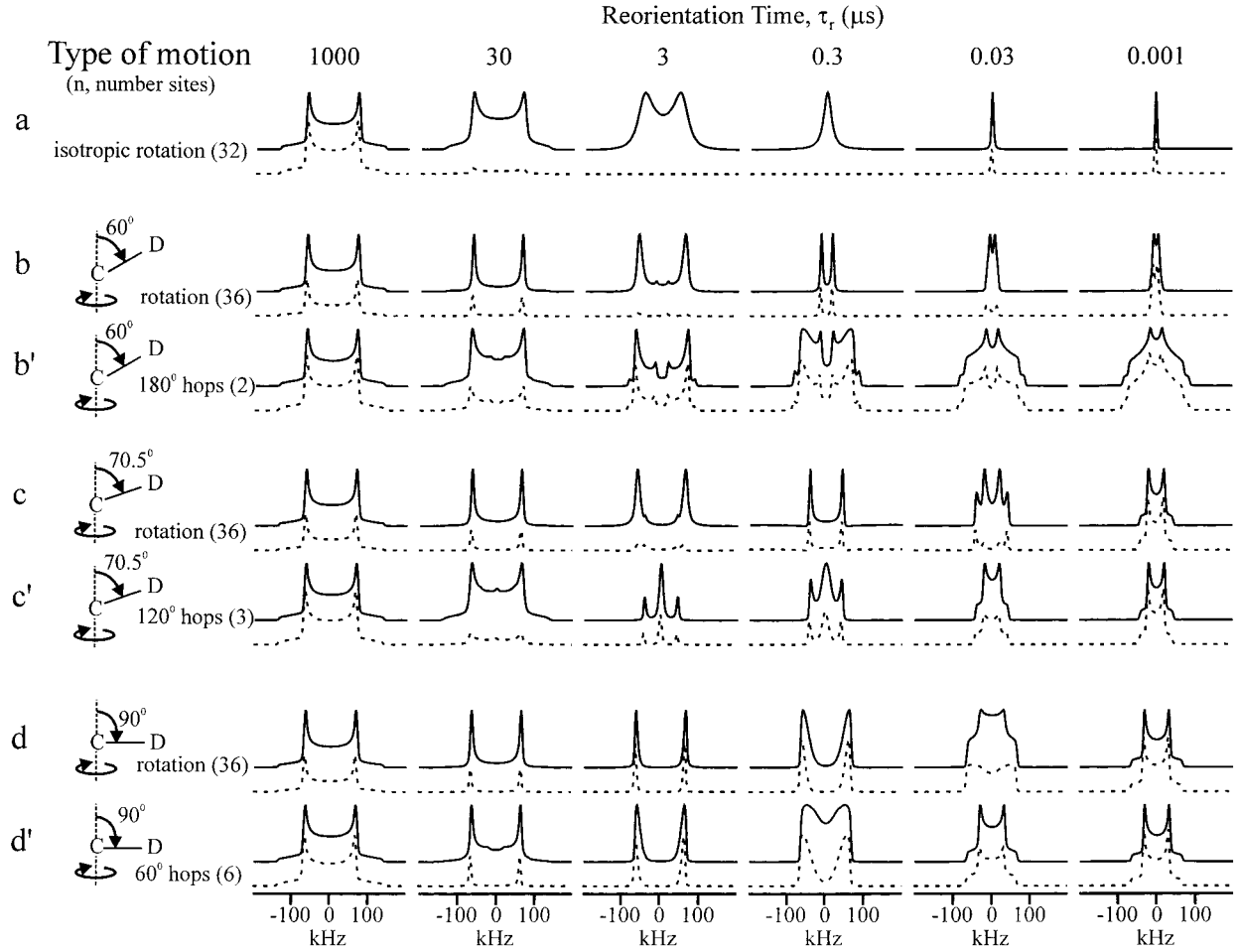

FIGURE 1. Computer simulated ^{2}H NMR line shapes for a C−^{2}H ≡ C−D moiety with Q_{cc} = 180 kHz and η = 0 for quadrupole-echo pulse spacing periods (t_q) of 40 μs (upper trace of each pair) and 100 μs (lower, dashed trace of each pair). Simulated spectra given for various motional models with correlation times (τ_r = average time to execute an angular reorientation of one radian) of 1000, 30, 3, 0.3, 0.03, and 0.001 μs, where $\tau_r = n\tau_j/(4\pi)$ for panels b, c, c′, d, and d′; for panel b′, $\tau_r = \tau_j/\pi$; and τ_r = 0.0199 τ_j for panel a.

this may not be the most "general" or "rigorous" way to average (or, in a sense, normalize) the characteristic times of all the types of motion that are simulated, it is a simple way and easily computed from the input parameters of the computer simulations. For motional models b, c, c′, d, and d′, $\tau_r = n\tau_j/(4\pi)$; for motional model b′, $\tau_r = \tau_j/\pi$; for isotropic reorientation (model a), τ_r = 0.0199τ_j. Comparison of the simulated line shapes for specific equal values of τ_r, as in Figure 1, (or, alternatively, for equal values of τ_j, not shown here) reveals that most line shapes based on corresponding models are qualitatively similar.

One can see in Figure 1 that, in general, the intensities of the patterns obtained for t_q = 40 μs are greater than or equal to those obtained for t_q = 100 μs; this reflects the additional unrefocused dephasing that occurs during the additional 2 × (100−40) = 120 μs dephasing period of the t_q = 100 μs case. One can see from the simulations displayed that the biggest spectral change in progressing from a quadrupolar echo period (t_q) of 40 to 100 μs occurs for a motional correlation time that is roughly comparable to these t_q values, i.e., τ_r = 3 or 30 μs in the cases examined.

Figure 1a shows a series of simulations for the case of isotropic reorientation, with various correlation times; this is actually accomplished in the computation by reorientation of the C−D vector among 32 orientations corresponding to the 32 lines between the center of an icosahedron and its 20 face centers and 12 vertexes. One sees that, for τ_r = 0.001 μs, isotropic reorientation yields the expected liquidlike spectrum. For intermediate correlation times (30, 3, or 0.3 μs), characteristic patterns are obtained for t_q = 40 μs. For t_q = 100 μs, the ^{2}H NMR intensity (relative to that for t_q = 40 μs) almost vanishes for τ_r = 0.3 and 3 μs, reflecting interference between motion and refocusing for this time period.

Figure 1, panels b and b′, represents the kind of situation one might expect for C−D moieties at C(2), C(3), C(5), and/or C(6) carbons of a planar six-membered (e.g., benzene) ring upon rotation or 180° ring flips, respectively, about the C(1)−C(4) internuclear axis. One can see that very rapid rotation (Figure 1b, τ_r = 0.001 μs) yields a Pake-type pattern that is dramatically collapsed (by a factor of 8). Intermediate rotational correlation times yield modified patterns. In contrast, much different and very distinctive ^{2}H NMR patterns are obtained from simulations for 180° flips about the motional axis (Figure 1b′).

Figure 1, panels c and c′, shows cases that correspond to the C−D moiety of a sp^3 carbon executing rotation or 120° "hops" (from the perspective of looking down along the motional axis), respectively. One sees that very rapid rotation or hops (τ_r = 0.001 μs) yields Pake-like patterns that are collapsed by a factor of 3. For intermediate τ_r values (30, 3, 0.3, or 0.03 μs), these types of motions yield different and distinctive patterns.

Figure 1, panels d and d′, shows the effects of rotation and 60° hops, respectively, about an axis that is oriented in a direction 90° from the C−D bond axis. This corresponds, for example, to rotation or hopping about the C_6 axis of a benzene ring. One can see that very rapid motion or rotation of these types yield Pake-like patterns that are collapsed by

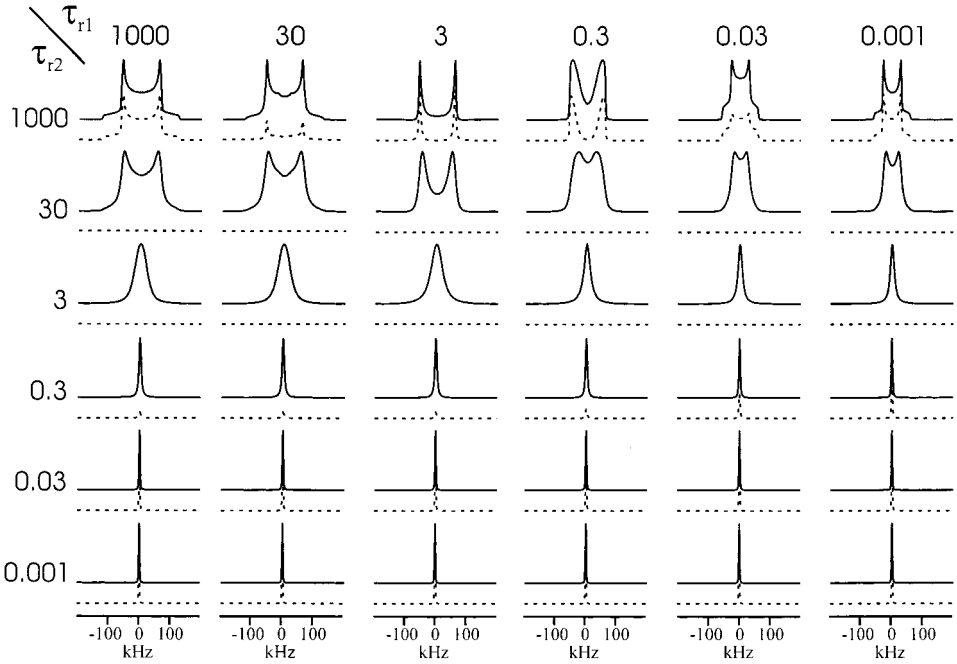

FIGURE 2. Computer simulated ^{2}H NMR line shapes for a C$-^2$H ≡ C−D moiety with Q_{cc} = 180 kHz and η = 0 for quadrupole-echo delay periods (t_q) of 40 μs (upper trace of each pair) and 100 μs (lower, dashed trace of each pair) for the model *a* case of two simultaneous motions described in the text. τ_{r1} values refer to three-site (120°) rotational jump motion about an axis $\mathbf{e}_r$, which reorients isotropically (represented by the 32-site icosahedron model) with a reorientational correlation time, τ_{r2}. The intensity of each line shape simulated for t_q = 100 μs is scaled relative to the corresponding t_q = 40 μs simulation. τ values in μs.

a factor of 2. Intermediate correlation times yield distinctive, partially averaged, patterns.

Some types of motion, which could be applicable to certain pollutant species adsorbed on a soil component (e.g., a clay or silica surface), cannot be described by simply one type of motion, as represented by the individual rows of line shapes in Figure 1, or even a superposition or sum of more than one type of motion, each occurring in a specific population of C−D moieties that does *not* interchange with the other population. These are motions in which two or more specific types of motion occur simultaneously, either (*a*) in the *same* population set or (*b*) in two different populations that interchange members between them. The existence of two (or more) *non*-exchanging populations and the type *b* situation are both consistent with the heterogeneous character of an intact soil or even of major soil components, e.g., a clay or humic.

An example of a situation of type *a* is given in Figure 2, which shows a series of simulations based on a system in which the C−D vector undergoes 3-fold rotational jumps (each of 120°) about an axis $\mathbf{e}_r$ that is perpendicular to the C−D axis, and with the axis $\mathbf{e}_r$ reorienting isotropically (as represented here in the 32-site icosahedron model described above) at a different rate (i.e., τ_{r1} for 3-fold jump rotation of the C−D axis ≠ τ_{r2} for isotropic reorientation of the $\mathbf{e}_r$ axis). This model might represent, for example, a pollutant molecule adsorbed on the surface of a small pore in the soil matrix (e.g., in/on a silica particle), executing rotational jump motion (characteristic time τ_{r1}) about an axis ($\mathbf{e}_r$) perpendicular to the pore surface at a specific point and periodically jumping (characteristic time τ_{r2}) to another site on the pore surface where it continues its rotational jump motion about a new axis, $\mathbf{e}_{r'}$.

Each row in Figure 2 shows a series of ^{2}H NMR line shapes corresponding to a range of reorientational correlation times (τ_{r1}) for the 3-fold "planar" rotational jump motion about a specific axis $\mathbf{e}_r$ (e.g., corresponding to a specific adsorption site of the pore) for a given value of the correlation time (τ_{r2}) for the isotropic reorientation of the $\mathbf{e}_r$ axis (e.g., corresponding to jumping to a different nearby adsorption site of the pore). The top row of Figure 2, which corresponds to very slow isotropic reorientation of the 3-fold rotation jump axis (τ_{r2} = 1000 μs), shows a range of simulated patterns that are, as expected, very similar to those given for 6-fold rotational jump motion in Figure 1d′. Each column of patterns in Figure 2 shows a series of ^{2}H NMR line shapes computed for various isotropic reorientation (e.g., adsorption site to adsorption site jump) correlation times (τ_{r2}) for a given rotational jump time (τ_{r1}) for each jump rotation axis, $\mathbf{e}_r$ (i.e., for each adsorption site). The left column of Figure 2, which corresponds to very slow 3-fold rotational motion (τ_{r1} = 1000 μs), shows a series of patterns that include the static Pake pattern at the top (τ_{r2} = 1000 μs) and the isotropically averaged narrow peak at the bottom (τ_{r2} = 0.001 μs), corresponding to the slow and fast limits, respectively. The patterns seen in the left column of Figure 2 are essentially the same as those shown for the isotropic reorientation model in Figure 1a. For simulated motions that correspond to intermediate values of both τ_{r1} and τ_{r2} (middle portions of the matrix of patterns), a variety of distinctive line shapes are seen. One of the most obvious patterns in Figure 2 is the fact that the intensities for the t_q = 100 μs patterns are extremely small for τ_{r2} values of 30 and 3 μs, relative to the corresponding t_q = 40 μs patterns.

Figure 3 shows a very simple example of case *b* specified above. In this example (model b_1), the C−D system undergoes exchange, at a rate corresponding to the correlation time τ_e, between the following two states: (A) a state in which the C−D vector undergoes infinitely rapid isotropic reorientation (simulated in the calculation by a site A that has the value zero for Q_{cc}) and (B) a completely static state. One can visualize situations in which a simple model of this type might represent important features of an adsorbed pollutant in a situation in which there is a rapid equilibrium between a tightly adsorbed, rigid state (B in the simple model, b_1) and a desorbed state (A in this model) in which the desorbed pollutant molecule is in a liquidlike state, perhaps in water-containing pores or in a nonaqueous-phase-liquid

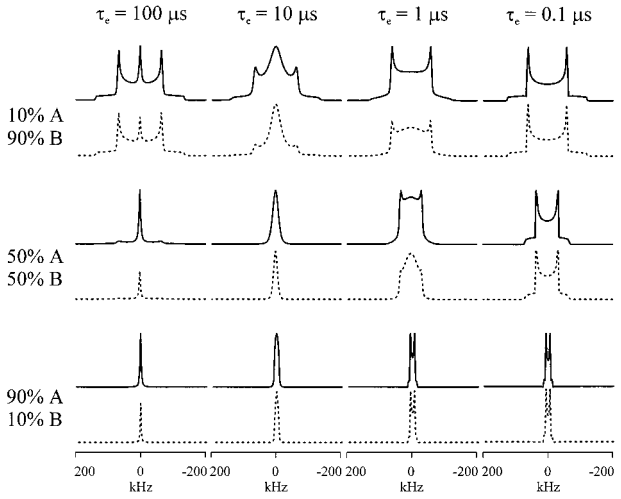

FIGURE 3. Computer simulated ^{2}H NMR line shapes for a C$-^2$H ≡ C−D moiety exchanging (exchange correlation time τ_e = 0.1, 1, 10, and 100 μs) between two sites: site A, with C−D moieties reorienting isotropically and infinitely rapidly (simulated by setting Q_{cc} = 0); site B, which is completely static, with Q_{cc} = 180 kHz. Two values of the quadrupole-echo pulse spacing period (t_q), 40 μs (upper trace of each pair) and 100 μs (lower, dashed trace of each pair), are represented.

(NAPL) pocket in the soil. The simulated patterns in Figure 3 reflect variations in both the populations P_A and P_B and the exchange parameter τ_e. These patterns cover a wide variety of shapes and widths.

The left column of patterns in Figure 3 represents a correlation time for exchange of 100 μs, which approaches the slow-exchange limit for this system. These patterns are essentially simple superpositions of the patterns expected for site A (corresponding to a liquidlike state, yielding the sharp peak in the middle) and for site B (corresponding to a completely rigid state, yielding a Pake-type pattern). For the 10% A/90% B mixture, these contributions are readily apparent in the simulated line shapes. However, because the total intensity of the B-site line shape is spread over a much broader pattern than for the narrow A-site line shape, the B-site contribution is much more difficult to see in the 50% A/50% B patterns shown in Figure 3 (especially for the t_q = 100 μs case) and impossible to detect in the 90% A/10% B case shown.

The right column of patterns in Figure 3 represents a correlation time for exchange of 0.10 μs, which approaches the fast-exchange limit for this system. In each case, one sees fully exchanged line shapes that are the *weighted averages* between the A-site patterns concentrated at the center of the pattern and the B-site Pake line shapes with horn-to-horn splittings of 135 kHz. For the 10% A/90% B case, this results in a Pake-type pattern that is scaled in width by the factor 9/10. For the 50% A/50% B case, the scaling factor is 5/10, and for 90% A/10% B, 1/10. For intermediate exchange rates (τ_e = 10 and 1.0 μs), Figure 3 shows a range of distinctive patterns.

The two states, A and B, in model b_1 are, of course, limiting cases that probably represent gross oversimplifications of most exchange situations that might be encountered in the types of experiments reported in this paper. A more realistic model of exchange between two different motional states would probably not be based entirely on two populations, in which one executes infinitely rapid motion and the other manifests infinitely slow motion over a large temperature range. An example of a model with exchange between two different populations, I and II, that would seem to be more realistic, at least in kind if not in detail, is represented by the simulations given in Figure 4. In this example (model b_2), the C−D system jumps (exchanges) between two different populations, I and II. The C−D moieties of population I undergo rotational 120° jump motion about a specific axis $\mathbf{e_r}$ that is perpendicular to the C−D bond axis, with a reorientational correlation time τ_{rI}. In population II, C−D units reorient isotropically, with a reorientational correlation time τ_{rII}. At first glance, it may appear that this motional model b_2 is very similar to model *a*. However, there are some important conceptual differences. One important difference is that in model b_2, for a specific crystallite or a small segment of the powder (with a specific orientation of the quadrupole tensor in space), the rotational jump component of motion always occurs about the *same* axis ($\mathbf{e_r}$) in contrast to the case of model *a* where $\mathbf{e_r}$ reorients isotropically. The model b_2 case could represent a situation in which a pollutant molecule adsorbed on a surface executes a rotational jump motion about an axis perpendicular to the adsorption site's surface and then periodically desorbs into a more mobile (isotropically reorienting state), subsequently adsorbing again at the original adsorption site.

Each row of ^{2}H NMR patterns in Figure 4 shows a series of line shapes computed for a range of reorientational correlation times (τ_{rI}) of the rotational jump motion about the axis $\mathbf{e_r}$ and corresponds to a given value of the correlation time (τ_{rII}) that characterizes isotropic reorientation of the desorbed species. Of course, in this model there is also a third correlation time that must be specified, namely, the correlation time, τ_e, that characterizes jumping between the two population sets. To keep the number of simulations within reason and to present the results in a comprehensible manner, we have arbitrarily limited the cases shown to those for which the correlation time (τ_e) for exchange between the population sets is taken to be proportional to the correlation time (τ_{rI}) for rotational jump motion about $\mathbf{e_r}$; specifically, we have imposed the condition $\tau_e = 40\pi/3 \times \tau_r = 10\tau_j$. While this imposed constraint cannot be justified here rigorously, the following plausibility argument for this *type* of constraint (assumption) can be advanced: The rotational jumps of a physisorbed (C−D)-bearing pollutant molecule about an axis ($\mathbf{e_r}$) perpendicular to the adsorption surface probably requires weakening of the same physisorption interactions that must be overcome for desorption. One can therefore imagine that, on the average, a certain fraction of the energetic activations that enable the rotational jumps also lead to desorption; in the present case, we arbitrarily assume that one-tenth of the 120° rotational jump processes lead to desorption. Another parameter that had to be included as input for the line shape simulations of Figure 4 is the ratio of populations of the two states. In the examples shown in Figure 4, we arbitrarily used the ratio, P_I/P_{II} = 3.

The patterns displayed in Figure 4 display some of the exchange features seen in the simpler exchange model b_1 represented in Figure 3. Each column of Figure 4 presents a series of ^{2}H line shapes simulated for a range (0.001−1000 μs) of correlation times (τ_{rII}) for isotropic reorientation of C−D moieties in population II, for a specific value of the correlation time (τ_{rI}) for 3-fold rotational jump motion of population I, and for a specific rate (specified by the correlation time, τ_e) for exchange jumps between the two populations. Each row of Figure 4 presents a series of ^{2}H line shapes simulated for a specific τ_{rII} value of population II for a range of τ_{rI} values of population I and a range of τ_e values for exchange between the two populations (with τ_e arbitrarily set to $10\tau_{jI}$ in this specific model, b_2).

The left column of this figure represents the effects of isotropic reorientational motion at various rates in population II for the slowest 3-fold rotational motion in population I (τ_{rI} = 1000 μs) and the slowest exchange ($\tau_e = 41.9 \times 10^3$ μs) between the two population sets. For τ_{rII} = 1000 μs, one sees

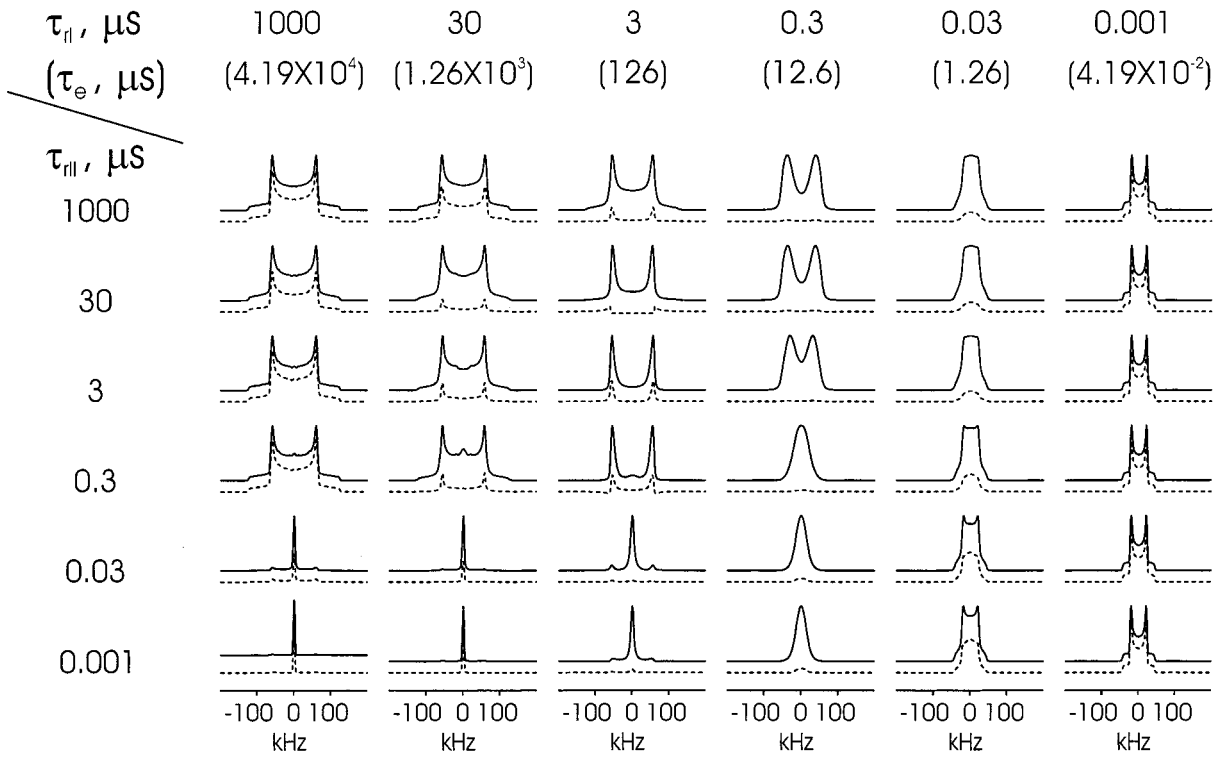

FIGURE 4. Computer simulated ^{2}H NMR line shapes for a C−^{2}H ≡ C−D moiety with Q_{cc} = 180 kHz and η = 0 for quadrupole-echo delay periods (t_q) of 40 μs (upper trace of each pair) and 100 μs (lower, dashed trace of each pair) for the model *b* case of rapid exchange between two populations. τ_{rI} values refer to three-site (120°) rotational jump motion in population I about an axis e_r. τ_{rII} is the correlation time for isotropic reorientation (32-site icosahedral model) in population II, with the exchange (jumps) between the two sites characterized by a correlation time τ_e, set according to the relationship $\tau_e = 40\pi/3 \times \tau_{rI}$. The populations were set at P_I/P_{II} = 3. The intensity of each line shape simulated for t_q = 100 μs is scaled relative to the corresponding t_q = 40 μs simulation.

in the left column the computed ^{2}H line shape patterns that are superpositions of identical Pake patterns corresponding to the 75% population I component and the 25% population II component. Moving down this left column, one sees the effects of increasingly rapid isotropic reorientation in the 25% population II component, while motion in the population I component remains slow ($\tau_{rI} = 1000\ \mu$s) and exchange between the populations remains slow ($\tau_e = 41.9 \times 10^3\ \mu$s). For $\tau_{rII} = 0.03$ and 0.001 μs, one sees the emergence of the motionally averaged contributions of population II in the form of a relatively sharp peak in the center superimposed on the Pake pattern due to population I (which is of low vertical amplitude in these line shapes because of the high amplitude of the sharp central peak). Hence, these patterns appear to be completely dominated by the sharp central peak.

The right column of Figure 4 shows the effect of variation of the correlation time (τ_{rII}) of the isotropic reorientational motion of population II for fast three-site rotational motion in population I ($\tau_{rI} = 0.001\ \mu$s) and for rather rapid exchange between the two populations ($\tau_e = 41.9 \times 10^{-3}\ \mu$s). These patterns represent averaging of the 75% weighted, motionally narrowed population I (essentially a Pake pattern that is scaled down in width by a factor of 2: Figure 1d′) and the 25% weighted, motionally narrowed population II (represented in Figure 1a for various τ_{rII} values). For the fastest population II motion represented in the right column of Figure 4 ($\tau_{r2} = 0.001\ \mu$s), the resulting exchange-averaged pattern reflects the 75% contribution of the 67.5 kHz horn-to-horn population I pattern (Figure 1d′, right column) and the 25% contribution of the isotropic averaged peak of population II (Figure 1a, right column); the result is a Pake pattern that is scaled down by the factor, 3/8. For the other entries in the right column of line shapes in Figure 4, including the line shape simulated for the slowest population II motion ($\tau_r = 1000\ \mu$s), the patterns are nearly the same as for the $\tau_{rII} = 0.001\ \mu$s case. This reflects the fact that the occurrence of relatively fast exchange (τ_e = 0.0419) for the systems represented in the right column effectively brings about rapid isotropic averaging of the population II component, although τ_{rII} = 1000 μs, because an exchange jump from each population I orientation of the C−D vector has an equal probability of jumping to any one of the 32 population II orientations. Combinations of intermediate values of the various correlation times yield patterns in Figure 4 that reflect gradations between these limiting behaviors.

Experimentally Determined ^{2}H Line Shape Patterns. Figure 5 shows a series of ^{2}H NMR spectra obtained on a sample of $HOCD_2CD_2OH$ adsorbed on dry Uncompahgre humic acid (3.9% loading). These spectra show the progression from the broad Pake-like pattern (~126 kHz splitting of the horns) of the essentially rigid molecule (at −125 °C) to the more rapidly reorienting case represented at the highest temperature examined. It is interesting that the ^{2}H line shape patterns of Figure 5 maintain a substantial component of essentially the full horn-to-horn width (~126 kHz) throughout most of the temperature range examined; yet almost any type of motion (including multi-axis motions of type *a* referred to above), if it is sufficiently fast to effect the shape of the ^{2}H pattern, also reduces its overall breadth (the exception among the cases shown in Figure 1 being the 180° hop motion of panel 1b′). Hence, it seems likely that a large fraction of the ethylene glycol molecules adsorbed on this humic acid remain substantially immobilized, even at temperatures as high as ~−25 °C. Simulations of these spectra and of other $HOCD_2CD_2OH$/substrate samples (with systematic variations of substrate, loading level, and moisture content) will be presented elsewhere (*12*).

Qualitatively similar patterns, albeit with more motion evident at lower temperatures, are seen in Figure 6, which

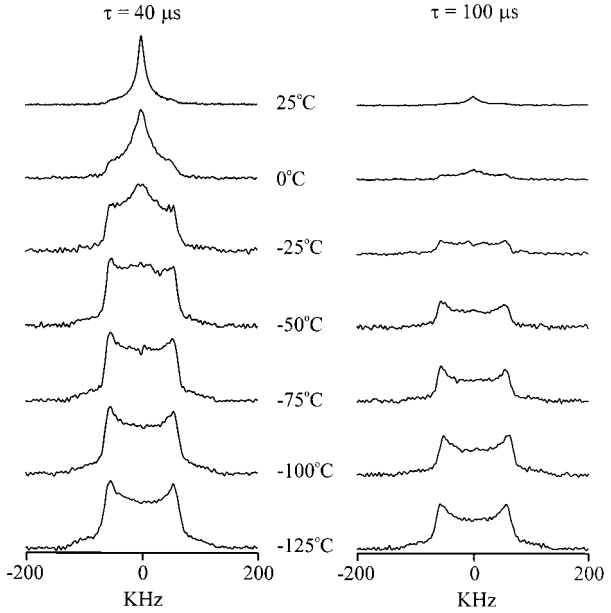

FIGURE 5. ^{2}H NMR spectra of a sample of $HOCD_2CD_2OH$ adsorbed on dry Uncompahgre humic acid (3.9% w/w loading level), as a function of temperature and quadrupole-echo delay period (t_q), as indicated.

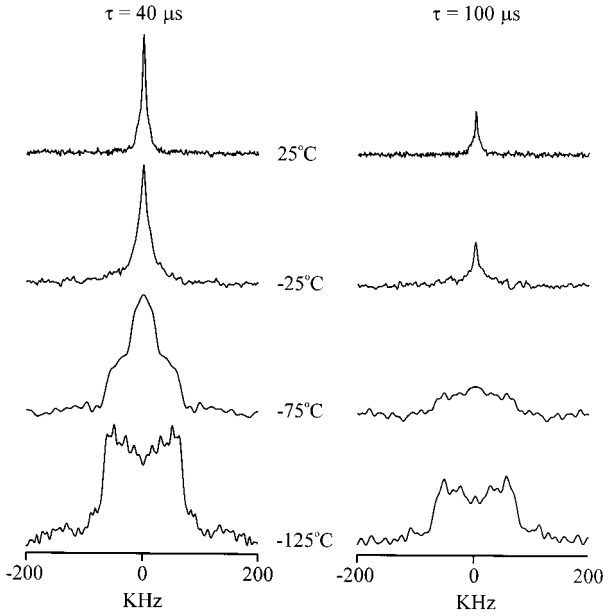

FIGURE 6. ^{2}H NMR spectra of a sample of $Cl_2C{=}CDCl$ adsorbed on Ca-montmorillonite (7.0% w/w loading level, ambient moisture), as a function of temperature and quadrupole-echo delay period (t_q), as indicated.

shows preliminary ^{2}H NMR spectra of a sample of $Cl_2C{=}CDCl$ adsorbed on a Ca-montmorillonite sample with ambient moisture; the loading level was 7.0 wt %. The spectra obtained at the lowest temperature examined (−125 °C) show a crude Pake-like pattern, albeit with a low S/N ratio that prevents unequivocal interpretation of its shape. Even above the −88 °C melting point of trichloroethylene (especially in the −75 °C spectrum), a large component of the "fully broadened" pattern is present. This indicates a strong interaction, yielding a nearly static species for the $Cl_2C{=}CDCl$/Ca-montmorillonite system, requiring thermal activation at temperatures substantially above the melting point before liquidlike motion can occur. The spectra obtained at 25 °C, and to a substantial degree at −25 °C, are dominated

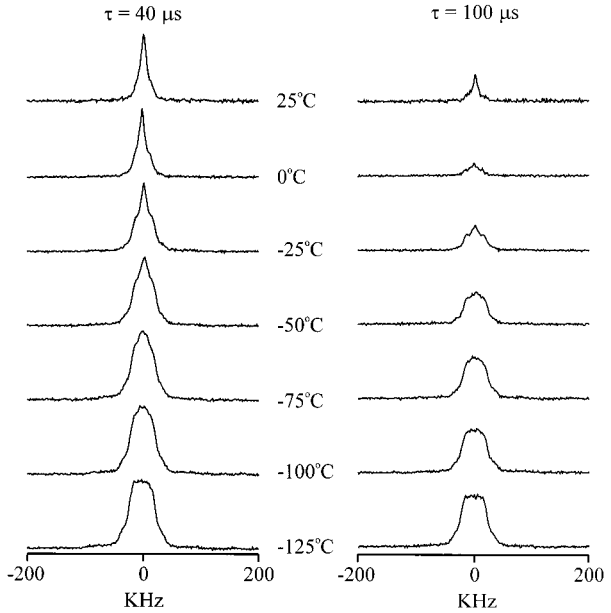

FIGURE 7. ^{2}H NMR spectra of a sample of $CD_3C(O)CD_3$ adsorbed on Ca-montmorillonite (1.8% w/w loading level on a dried clay), as a function of temperature and quadrupole-echo delay period (t_q), as indicated.

by the sharp central peak that results from rapid and largely isotropic reorientation with a residual broad contribution due to a component with more constrained motion (most evident in the low S/N, broad component in the spectrum obtained at −25 °C with a quadrupolar echo delay of 100 μs).

Figure 7 shows ^{2}H NMR spectra obtained on a sample of $CD_3C(O)CD_3$ adsorbed on Ca-montmorillonite (1.8% loading level on a dry clay). These spectra show a progression from a relatively broad pattern at the lowest temperature (−125 °C) to a substantially sharpened peak at 25 °C, which still retains a substantial peak width (much broader at half-height than that of $Cl_2C{=}CDCl$/Ca-montmorillonite at 25 °C). The −125 °C spectrum is narrowed by roughly a factor of 3 relative to the width of a corresponding static sample Pake pattern (e.g., $HOCD_2CD_2OH$/humic or $Cl_2C{=}CDCl$/Ca-montmorillonite at −125 °C, in Figures 5 and 6). This *width* is consistent with rapid rotation of the CD_3 group about the C−C bond axis, as represented in the simulations in Figure 1, panels c and c′. However, there is no evidence in the spectra of Figure 7 of the horns (sharp, intense features) in Figure 1, panels c and c′; this implies an additional broadening contribution to the pattern, possibly due to a distribution of states and motions in the sample. In addition to the absence of distinct horns in the −125 °C spectrum, one also sees a substantial intensity in the central region of the spectrum. This combination of features can be reproduced qualitatively in simulations (not shown here) of a composite motion consisting of three-site hop/rotation of the CD_3 group about the C−C axis and two-site (C_2) hops about the C=O axis. The key feature of such simulations that fit the experimentally observed patterns satisfactorily is that the 180° hops be rapid ($\tau_r \leq 0.01$ μs). This kind of motion can be envisioned as occurring in a hydrogen-bonded complex of the type $(CD_3)_2C{=}O\cdots HA$), where HA represents an "acidic" site on the clay surface. The line narrowing that occurs at higher temperatures can be due to some combination of additional motional narrowing (e.g., freer rotation about the C=O bond axis in a hydrogen-bonded complex) and exchange between a less mobile acetone state (e.g., with 180 °C_2 hops and −CD_3 rotation) and an isotopically reorienting state. The spectra obtained on the $CD_3C(O)CD_3$/Ca-montmorillonite sample are to some degree (at a quantitative level) tainted by the

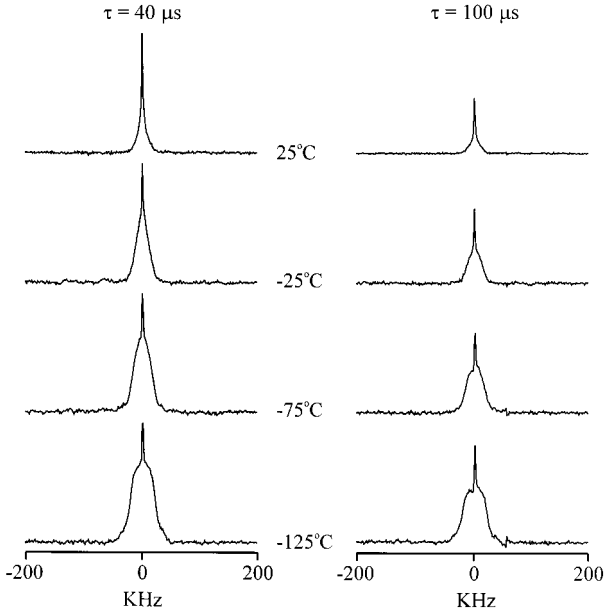

FIGURE 8. ^{2}H NMR spectra of a sample of $CD_3C(O)CD_3$ adsorbed on Uncompahgre humic acid (6.5% w/w loading level, ambient moisture), as a function of temperature and quadrupole-echo delay period (t_q), as indicated.

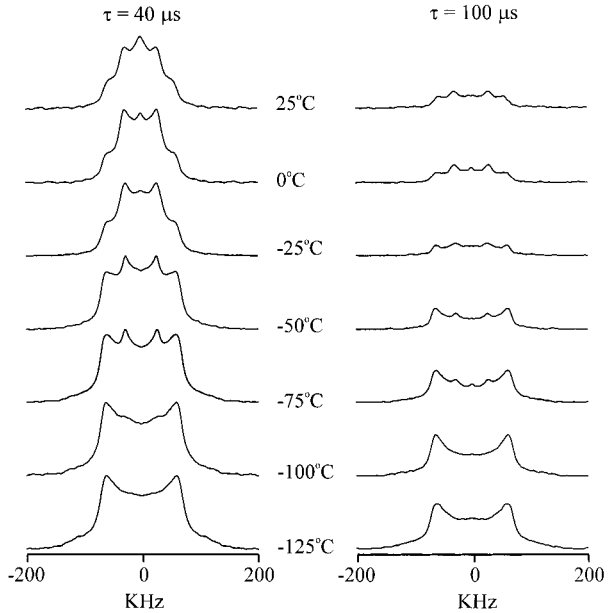

FIGURE 9. ^{2}H NMR spectra of a sample of C_5D_5N (perdeuteriopyridine) adsorbed on Ca-montmorillonite (2.0% w/w loading level, ambient moisture), as a function of temperature and quadrupole-echo delay period (t_q), as indicated.

possibility of ^{2}H for ^{1}H exchange with the clay protons. Mass spectral results showed this exchange to be significant but not dominant; nevertheless, the ^{2}H pattern should contain a small contribution from ^{2}H on Ca-montmorillonite.

Figure 8 shows the ^{2}H line shapes obtained experimentally on a sample of $CD_3C(O)CD_3$ adsorbed on Uncompahgre humic acid (ambient moisture content, 6.5% loading level). All of the spectra, even those obtained at −125 °C, show a sharp component superimposed on a broad component, corresponding to two separate populations, between which any exchange is not very fast. The broad component is, for the lower temperatures, nearly superimposable on the corresponding broad patterns seen in Figure 7. Hence, one might infer that the kind of population giving rise to this component of the line shape is present in both types of systems (samples). The fact that the higher temperature patterns in Figure 8 are so much narrower than those of Figure 7 at corresponding temperatures may reflect a much higher fractional population of an isotropically reorienting component in the $CD_3C(O)CD_3$/humic sample than in the $CD_3C(O)CD_3$/Ca-montmorillonite sample as well as a smaller τ_r value for the isotropically reorienting acetone molecules in the sample of Figure 8. The gradual narrowing of the pattern as the temperature is increased is consistent with the enhanced importance of isotropic reorientation at the highest temperatures. Of course, ^{1}H−^{2}H exchange can also occur in this system. Also, it is clear that there is a much larger component of isotropic reorientation in the $CD_3C(O)CD_3$/humic sample than in the $CD_3C(O)CD_3$/Ca-montmorillonite sample. At higher temperatures this could conceivably be due, at least partly, to ^{2}H resonances from HOD resulting from ^{1}H−^{2}H exchange. However, at low temperatures, HOD would be frozen, yielding a very broad ^{2}H NMR pattern where the narrow component could be due to rotating, isolated acetone molecules that are trapped in small voids in the humic acid.

The ^{2}H NMR spectra obtained on a sample of C_5D_5N (perdeuteropyridine) adsorbed on Ca-montmorillonite (ambient moisture content, 2% loading level) are shown in Figure 9. These spectra display the complexity one might expect for a perdeuterated species with more than one site in each molecule and perhaps more than one component (from the motional point of view) in the sample. All of the spectra shown in Figure 9, even those obtained at 25 °C, have a substantial broad component. In the case of pyridine adsorbed on a substrate with acidic sites, one might expect at least some contributions from hydrogen-bonded complexes of the type I.

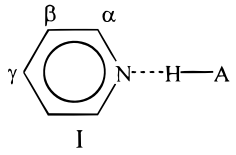

I

Motion about the $C_\gamma\cdots N\cdots H$ (hydrogen-bond) axis will leave the $C-D_\gamma$ moiety unchanged, but will cause the $C-D_\alpha$ and $C-D_\beta$ moieties to reorient according to the situations represented, for example, by Figure 1, panels b and b′. Thus, even a single motional component can yield a superposition of at least two line shape patterns (one for $C-D_\gamma$ and one for $C-D_\alpha$ and $C-D_\beta$).

The ^{2}H line shape patterns seen for the lowest temperature represented in Figure 9 (−125 °C) are dominated by the rigid powder pattern (Figure 1a) expected when all motion is very slow. As the temperature of the C_5D_5N/Ca-montmorillonite sample is increased, one sees the growth of additional motional components. At −75 °C one sees a distinct contribution due to a motion that reduces the "splitting between horns" by roughly a factor of about 2.5; this pattern can be simulated for $C_\alpha-D$ and $C_\beta-D$ by 180° flips about the $C_\gamma\cdots N\cdots H$ axis (Figure 1b′).

As the temperature of the C_6D_5N/Ca-montmorillonite sample is increased above −75 °C, the ^{2}H line shapes show an enhanced contribution from the narrower Pake-like pattern and a decreasing contribution from the broader Pake-like pattern, as populations of the corresponding components adjust accordingly. At the higher temperatures examined, one also sees a growing contribution from a central peak that presumably represents a growing population of a component that reorients increasingly isotropically. These higher temperature results show some substantial similarities to results obtained on C_5D_5N adsorbed in a coal (*6*), which

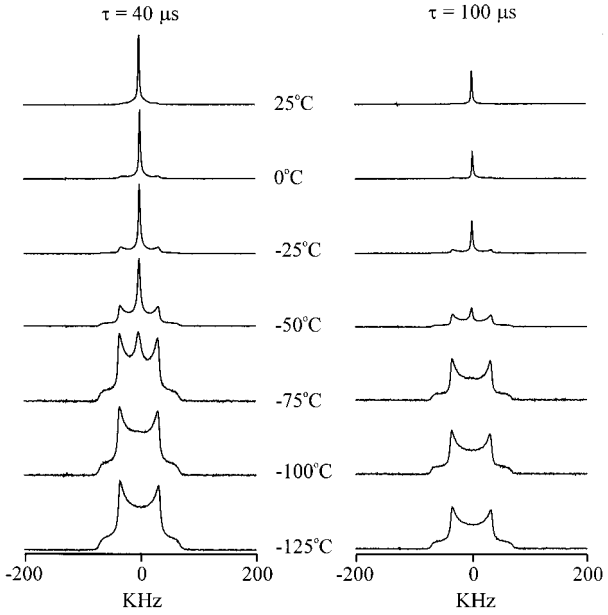

FIGURE 10. ^{2}H NMR spectra of a sample of C_6D_6 adsorbed on Ca-montmorillonite (3.9% w/w loading level, dry), as a function of temperature and quadrupole-echo delay period (t_q), as indicated.

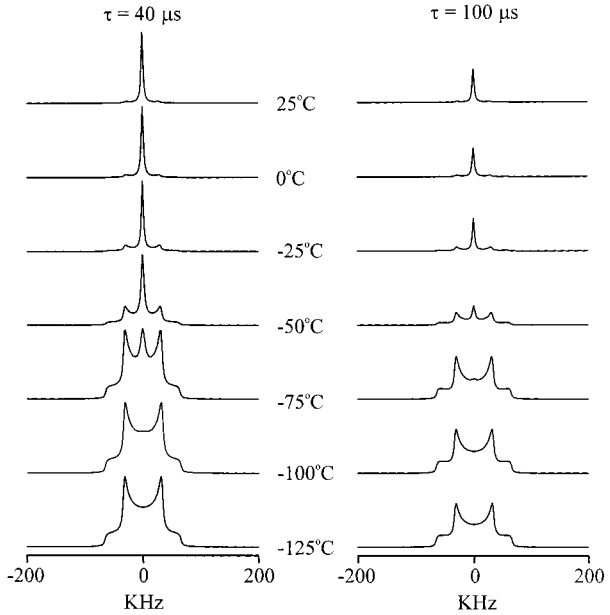

FIGURE 11. Computer simulations of the ^{2}H NMR spectra of Figure 10, based on the two-state model, with populations $P_{iso} = P_C$ and $P_D = 1 - P_C$ given in Table 1, and with no exchange between the states. In state C, the benzene molecules undergo extremely fast rotational motion about the C_6 axis, and the C_6 rotational axis undergoes isotropic reorientation (with a correlation time, τ_1). In state D, the benzene molecules undergo rotation about the C_6 axis (simulated by jumps among three sites, with a correlation time, τ_2); the C_6 axis undergoes diffusional motion (simulated by jumps along the surface of a cone, defined by the half angle, ϕ; 10 jump sites, with a correlation time, τ_3).

were explained on the basis of a superposition of two types of motion about the N···H axis, *b*-type and *b′*-type motions in Figure 1. Detailed simulations on the spectra in Figure 9 of the ^{2}H line shapes obtained on numerous C_5D_5N/substrate samples (in which the substrate, loading level, and moisture content were varied systematically) will be presented elsewhere (*11*).

Figure 10 shows ^{2}H NMR spectra obtained on a sample of C_6D_6 adsorbed on Ca-montmorillonite (dry, 3.9% loading level). The line shapes shown in Figure 10 do not display, even at the lowest temperature examined (−125 °C), a contribution from a Pake-like pattern similar to the broader one seen in the C_5D_5N/Ca-montmorillonite case in Figure 9. In this C_6D_6/Ca-montmorillonite case, only a narrower Pake-like pattern, presumably resulting from rapid rotation about the C_6 axis (Figure 1d), is evident. As the temperature of the C_6D_6/Ca-montmorillonite sample is increased, increasingly rapid and random reorientation of the C_6 rotation axis occurs, ultimately yielding an increasingly narrowed spectrum at the highest temperature.

Figure 11 presents the results of computer simulations of the experimental spectra shown in Figure 10. These simulations are based on a model consisting of two components, C and D, between which there is no exchange. In component C, which has a dominant population at 25 °C, the benzene molecules execute extremely rapid ($\tau = 0$) rotational motion about benzene's C_6 axis. This C_6 axis undergoes isotropic reorientation, which in this case is simulated by jumps between 14 sites on the vertexes and face centers of a cube, with correlation time, τ_1. In state D, the benzene molecules execute rotation about the C_6 axis (simulated by jumps among three sites, with a correlation time, τ_2); the C_6 rotational axis undergoes a wobble that is simulated by a diffusional model of jumps among 10 orientations of the C−D vector (correlation time, τ_3) on a cone defined by the half angle ϕ. According to this model, as the wobbling-rotating, adsorbed benzene molecules (D) desorb from the surface, their C_6 axis rotation becomes unhindered and extremely fast, while the wobbling motion of the C_6 axis turns into the isotropic reorientational motion of state C. The input parameters of this model, which are summarized in Table 1, were varied to fit the ^{2}H line shape at each temperature. For example, the population of state C varies between 87% (0.87) at 25 °C to 0% at −125 °C. The cone angle ϕ varies between about 20° at 25 °C and about 5° at −125 °C.

TABLE 1. Summary of Parameters for Computer Simulation of ^{2}H NMR Line Shapes in Figure 11

temp (°C)[a]	ϕ (deg)[b]	k_{iso} (s^{-1})[c]	k_{wob} (s^{-1})[d]	k_{rot} (s^{-1})[e]	P_{iso} [f]
25	20.0	4.2×10^5	1.0×10^5	2.7×10^7	0.87
0	17.5	3.5×10^5	1.0×10^5	2.7×10^7	0.86
−25	15.0	4.2×10^5	1.0×10^5	2.7×10^7	0.68
−50	12.0	2.2×10^5	1.0×10^5	2.7×10^7	0.60
−75	10.0	1.2×10^5	8.0×10^4	2.0×10^7	0.39
−100	7.5	6.5×10^4	6.0×10^4	1.8×10^7	0.23
−125	5.0		3.0×10^4	1.8×10^7	0.00

[a] Sample temperature corresponding to the experimental spectrum in Figure 10 that is simulated in Figure 11. [b] The angle ϕ that defines the half-angle of the wobble cone of component D. [c] $k_{iso} = \tau_1^{-1}$ for the isotropically reorienting component C. [d] $k_{wob} = \tau_3^{-1}$ for the wobbling motion of component D. [e] $k_{rot} = \tau_2^{-1}$ for the three-site jump around the C_6 axis of benzene in component D. [f] Fractional population of the isotropically reorienting state, C.

The simulations summarized in Figure 11 and Table 1 provide estimates of populations ($P_{iso} \equiv P_C$; $P_D \equiv 1 - P_C$) and motional rate constants ($k_{iso} = \tau_1^{-1}$; $k_{rot} = \tau_2^{-1}$; and $k_{wob} = \tau_3^{-1}$) used to simulate the experimental line shapes of Figure 10 over a range of temperatures from −125 to 25 °C. From the simulation parameters required to fit the spectra over this temperature range, one obtains at least a crude measure of the temperature dependences of these motional rate constants and of the equilibrium constant, $K = P_C/P_D$. Then, from a simple Arrhenius expression for each rate constant, $k = A \exp[-E_a/RT]$, one can estimate the activation energy, E_a, for each type of motion. In this way (neglecting data points corresponding to rate constants so large that the line shapes cannot distinguish modest variations), one obtains the following estimates: $\Delta E_a = 6.4 \pm 0.6$ kJ mol^{-1} for isotropic

reorientation of the C_6 axis in population C, $\Delta E_a = 1.6 \pm 0.5$ kJ mol^{-1} for the C_6 rotation in population D and $\Delta E_a = 4.4 \pm 0.4$ kJ mol^{-1} for the wobbling motion in population D. Similarly, applying the van't Hoff equation, d (ln K)/d ($1/T$) $= -\Delta H°/R$, to the temperature dependence of populations estimated in Table 1, one obtains the following estimates for the process, D $\rightleftarrows$ C: $\Delta H° = 11.2 \pm 0.8$ kJ mol^{-1} and $\Delta S° = 54 \pm 5$ J K^{-1} mol^{-1}. The latter seems reasonable for what appears to be essentially the desorption of benzene from a clay surface, while the former indicates that the benzene−clay interaction in the adsorbed state (D) is weak.

Conclusions

^{2}H NMR line shapes show a variety of patterns and temperature dependences for various samples consisting of a deuterated pollutant adsorbed on a soil component as a substrate. These line shapes can be understood in terms of models of the local motion of C−D moieties. Computer simulations of experimental results can provide a means of elucidating the details of the local motion, including the relevant motional correlation time(s), from which motional activation energies can be calculated from their temperature dependences. This approach, which can be implemented straightforwardly with widely available equipment and techniques, shows great promise for elucidation of an extremely important aspect of the fundamental behaviors of pollutant species adsorbed in soils.

Acknowledgments

The authors gratefully acknowledge support of this work by DOE Grant DE-FG-03-95ER14558 and AFOSR Grant F49620-95-1-0192 and R. R. Vold for providing the simulation program, MXET1. We also thank Dr. Jane Yang, who prepared some of the samples.

Literature Cited

(1) Spiess, H. *Adv. Polym. Sci.* **1985**, *66*, 23.

(2) Jelinski, L. W. *Annu. Rev. Mater. Sci.* **1985**, *15*, 359.

(3) Barbara, T.; Greenfield, M. S.; Vold, R. L.; Vold, R. R. *J. Magn. Reson.* **1986**, *68*, 311.

(4) Hirschinger, J.; English, A. D. *J. Magn. Reson.* **1989**, *85*, 542.

(5) Ziegler, R. C.; Maciel, G. E. *J. Am. Chem. Soc.* **1991**, *113*, 6349.

(6) Jurkiewicz, A.; Frye, J. S.; Maciel, G. E. *Fuel* **1990**, *69*, 1507.

(7) Keeler, C.; Maciel, G. E. To be published.

(8) Davis, J. H.; Jeffrey, K. R.; Bloom, M.; Valic, M. I.; Higgs, T. P. *Chem. Phys. Lett.* **1976**, *42*, 390.

(9) Boden, N.; Clark, L. D.; Hanlon, S. M.; Mortimer, M. *Faraday Symp. Chem. Soc.* **1978**, 109.

(10) Greenfield, M. S.; Ronemus, A. D.; Vold, R. L.; Vold, R. R.; Ellis, P. D.; Raidy, T. E. *J. Magn. Reson.* **1987**, *72*, 89−107.

(11) Xiong, J.; Chuang, I-S.; Lock, H.; Maciel, G. E. *J. Phys. Chem.* To be submitted.

(12) Keeler, C.; Xiong, J.; Lock, H.; Maciel, G. E. *J. Phys. Chem.* To be submitted.

Received for review November 30, 1998. Accepted April 16, 19991999.

ES981221WES981221W